C. R. Mecanique 343 (2015) 680–688

Contents lists available at ScienceDirect

Comptes Rendus Mecanique

www.sciencedirect.com

Acoustic metamaterials and phononic crystals

Quasistatic stopband and other unusual features of the spectrum of a one-dimensional piezoelectric phononic crystal controlled by negative capacitance

Anton A. Kutsenko [a,b], Alexander L. Shuvalov [a,b], Olivier Poncelet [a,b,*], Alexander N. Darinskii [c]

[a] Univ. Bordeaux, I2M-APY, UMR 5295, 33405 Talence, France
[b] CNRS, I2M-APY, UMR 5295, 33405 Talence, France
[c] Institute of Crystallography RAS, 119333 Moscow, Russia

ARTICLE INFO

Article history:
Received 24 March 2015
Accepted 9 July 2015
Available online 17 August 2015

Keywords:
Tunable phononic crystals
Piezoelectric structures
Electric control
Negative capacitance
Quasistatic stopband

ABSTRACT

Normal propagation of the longitudinal wave through the piezoelectric medium with periodically embedded electrodes is considered. Each pair of electrodes is connected via a circuit with capacitance C. The paper analyzes in detail the unusual features of the dispersion spectrum $\omega(KT)$ (K is the Floquet–Bloch wavenumber, T is the period) arising in the special case of a negative value of C. The solution of the dispersion equation shows explicitly the evolution of the passbands and stopbands tunable by varying $C < 0$. One of the striking features is the existence of the poles of $\mathrm{Im}KT$ (infinite attenuation) and of the corresponding jumps of the phase $\mathrm{Re}KT$ from 0 to π in the stopbands for a certain range (C_0, C_1) of negative C. Besides, for $C \in (C_0, C_\infty)$ where $C_\infty < C_1$, the spectrum possesses a low-frequency absolute stopband starting from the quasistatic limit $\omega = 0$ and including the tunable pole of $\mathrm{Im}KT$ inside. This stopband is related to the negative value of the quasistatic effective elastic constant in the range (C_0, C_∞). At $C = C_\infty$, the effective constant is infinite while the spectrum degenerates to the straight line $K = 0$ at any ω. For C close to C_∞, the spectrum consists of the branches with high group velocity and of the quasiflat branches.

1. Introduction

During the last decade, many ways of tuning the band diagrams of phononic crystals (PC) have been investigated. They mostly rely on the application of an external field stimulus (heat, magnetic or electric field, mechanical stress...) that modifies either the constitutive parameters of the PC components or their geometry [1–6]. Also, specifically for waveguides, the use of piezoelectric patches connected with appropriate electric circuits has shown a certain efficiency for tuning the band-diagrams [7–9]. More recently, other works have envisaged a different approach based on bulk control of the propagation with no external stimuli, but with thin embedded charged electrodes implying jumps of the electric induction and therefore jumps of the strain field across the electrodes [10–14]. Hence, controlling the charges within the electrodes with an appro-

* Corresponding author.
E-mail addresses: aak@nxt.ru (A.A. Kutsenko), alexander.shuvalov@u-bordeaux.fr (A.L. Shuvalov), olivier.poncelet@u-bordeaux.fr (O. Poncelet), alexandre_dar@mail.ru (A.N. Darinskii).

http://dx.doi.org/10.1016/j.crme.2015.07.005
1631-0721/

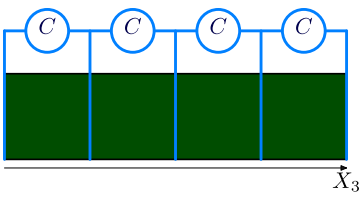

Fig. 1. (Color online.) Structure of the piezoelectric phononic crystal under consideration.

priate external impedance allows one to control efficiently the induced band diagrams of the structure with a tuning rate that is much higher. Specifically, Refs. [10–14] have considered the propagation of the longitudinal wave through a periodic structure of electrodes embedded into an elastic/piezoelectric multilayer or a homogeneous piezoelectric material. The connection of the electrodes via external electric circuits with the capacitance C enables the tunability of the wave properties. The dispersion equation for the cases of single-layered or bilayered unit cell has been obtained in [10,11] and generalized for the case of arbitrary multilayered unit cell in [12]. The dynamical effective constants of the periodic structure were derived in [12]. The papers [10–12] have dealt with positive C. At the same time, as it has been noted in [10,11], the capacitance C of the external circuit may be negative. A negative capacitance can be created electronically, for instance using negative impedance converters built of the so-called current conveyors (see [15,16]). Such devices have being increasingly used in the context of active vibration control and sound transmission loss [16–20]. The tunability of the elastic/piezoelectric PC using an external circuit with $C < 0$ has been preliminary considered in [13,14]. In particular, it has been shown in [13] and confirmed in [14] that negative values of C can create the low-frequency stopband starting from the quasistatic limit $\omega = 0$.

The present paper provides a complete analysis of the unusual spectral features that are made possible by the negative capacitance C of the external circuits connecting the electroded interfaces of the piezoelectric layers. For the sake of transparency, the case of periodic structure of identical electroded piezoelectric layers (single-layered unit cell) is considered. The tunability of the passbands and stopbands of the dispersion spectrum $\omega(KT)$ (K is the Floquet–Bloch wavenumber, T is the period) by means of varying $C < 0$ is described explicitly. It is shown that there is a certain range (C_0, C_1) of negative C for which the stopbands contain the poles of $\mathrm{Im}KT$ (infinite attenuation) and the corresponding jumps of the phase $\mathrm{Re}KT$ from 0 to π. The poles appear one by one as C decreases from C_0 to a certain critical value $C_\infty < C_1$ and then successively disappear as C further decreases from C_∞ to C_1. At $C = C_\infty$, the whole spectrum degenerates to the straight line $K = 0$ at any ω. For C close to C_∞, the spectrum consists of the branches with high group velocity and of the quasiflat branches. Besides, for $C \in (C_0, C_\infty)$ the spectrum possesses a broad quasistatic stopband starting at $\omega = 0$ and including the tunable pole of $\mathrm{Im}KT$ inside. This stopband is related to the negative value of the quasistatic effective elastic constant in the range (C_0, C_∞).

The paper is organized as follows. The background of the problem is provided in Section 2. It is shown that despite the 4×4 size of the initial piezoelectric propagator matrix, the dispersion spectrum $\omega(KT)$ can be described via the 2×2 propagator acting on the elastic state vector. Section 3 discusses unusual features in the evolution of the dispersion spectrum for an arbitrary piezoelectric material as C decreases from zero. Section 4 presents numerical examples for a PZT material. Concluding remarks are mentioned in Section 5.

2. Background

Consider a pure longitudinal time-harmonic wave propagating through the transversely isotropic piezoelectric medium along the principal axis X_3 perpendicular to the periodically embedded infinitely thin electrodes that are connected via the external capacitance C, see Fig. 1. Denote the mass density, the elastic constant at constant electric field, the elastic constant at constant electric induction, the piezoelectric constant and the dielectric constant at constant strain, respectively, by

$$\rho,\ c_{33}^{\mathrm{E}} \equiv c^{\mathrm{E}},\ c_{33}^{\mathrm{D}} \equiv c^{\mathrm{D}} = c^{\mathrm{E}} + e^2/\varepsilon,\ e_{33} \equiv e,\ \varepsilon_{33}^{S} \equiv \varepsilon$$

We will omit the indices of the traction and of the elastic and electric displacements, so that $\sigma_{33} \equiv \sigma$, $u_3 \equiv u$, $D_3 \equiv D$. Denoting the electric potential by φ, the governing equations in the piezoelectric medium regardless of the boundary conditions are

$$\begin{aligned} &\sigma' = -\rho\omega^2 u,\ D' = 0 \\ &\sigma = c^{\mathrm{E}} u' + e\varphi',\ D = eu' - \varepsilon\varphi' \end{aligned} \tag{1}$$

where $' = \mathrm{d}/\mathrm{d}z$ and z is the coordinate along X_3. Equations (1) may be cast as

$$\boldsymbol{\eta}' = \mathbf{Q}\boldsymbol{\eta} \quad \text{with } \boldsymbol{\eta} = \begin{pmatrix} u \\ \varphi \\ \sigma \\ D \end{pmatrix},\ \mathbf{Q} = \begin{pmatrix} 0 & 0 & 1/c^{\mathrm{D}} & e/\varepsilon c^{\mathrm{D}} \\ 0 & 0 & e/\varepsilon c^{\mathrm{D}} & -c^{\mathrm{E}}/\varepsilon c^{\mathrm{D}} \\ -\rho\,\omega^2 & 0 & 0 & 0 \\ 0 & 0 & 0 & 0 \end{pmatrix} \tag{2}$$

Note that we have defined $\mathbf{Q}$ as real. If there are no electrodes between the initial a and end points b, then the solution of (2) is

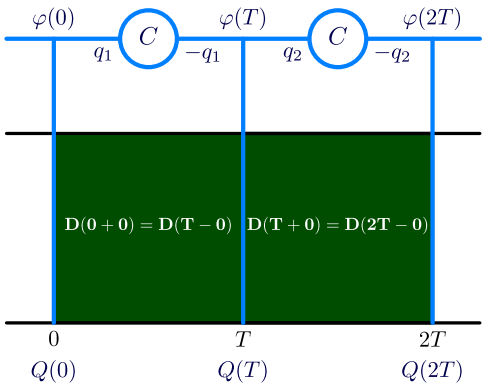

Fig. 2. (Color online.) Schematic view of the electrical connections of two piezoelectric layers with external capacitors within the unit cell.

$$\boldsymbol{\eta}(b) = \mathbf{M}_{4\times4}[b,a]\boldsymbol{\eta}(a), \quad \text{where } \mathbf{M}_{4\times4}[b,a] = \exp((b-a)\mathbf{Q}) \tag{3}$$

In particular, if $a=0$ and $b=T$ with T being the period, then the corresponding transfer matrix is called the monodromy matrix $\mathbf{M}_{4\times4} \equiv \mathbf{M}_{4\times4}[T,0]$. It has the following structure [21] (with the corresponding values for the homogeneous medium case):

$$\mathbf{M}_{4\times4} = \begin{pmatrix} M_{11} & 0 & M_{13} & M_{14} \\ M_{21} & 1 & M_{14} & M_{24} \\ M_{31} & 0 & M_{11} & M_{21} \\ 0 & 0 & 0 & 1 \end{pmatrix}, \quad \begin{cases} M_{11} = \cos kT,\ M_{21} = h(M_{11}-1),\ M_{13} = \dfrac{\sin kT}{Z} \\ M_{14} = hM_{13},\ M_{31} = -Z\sin kT,\ M_{24} = \dfrac{h\varepsilon M_{14} - T}{\varepsilon} \\ k = \omega\sqrt{\rho/c^{\mathrm{D}}},\ h = e/\varepsilon,\ Z = \omega\sqrt{\rho c^{\mathrm{D}}} \end{cases} \tag{4}$$

In order to obtain the transfer matrix $\mathbf{M}_{4\times4}[b,a]$, one should put $b-a$ instead of T in (4).

In addition to Eq. (3), the electrical network of capacitors brings the following periodic boundary conditions, here expressed for the electrode at $z=T$:

$$\begin{cases} C(\varphi(0) - \varphi(T)) = q_1 \\ C(\varphi(T) - \varphi(2T)) = q_2 \\ q_2 - q_1 + Q(T) = 0 \\ D(T+0) - D(0+0) = Q(T)/S \end{cases} \tag{5}$$

where q_1, q_2 are the charges on the capacitors connected to the electrode at $z=T$, Q is the charge on the electrode and S is its surface area, see Fig. 2. Note that equations (5) correspond, respectively, to: the voltage/charge relationship of the capacitances C; the conservation of charges over the two capacitors and the electrode; and the Gauss law expressed at the electrode. Equations (5) lead to

$$F(0) \equiv \frac{S}{C}D(+0) + \varphi(0) - \varphi(T) = F(T) \equiv \frac{S}{C}D(T+0) + \varphi(T) - \varphi(2T) \tag{6}$$

Equation (6) shows that the function F has the same value on each electrode nT. Using the second line of (3) with $[a,b] = [0,T]$ and (4), (6) we find

$$D(0) = \frac{M_{21}u(0) + M_{14}\sigma(0) + F(0)}{\frac{S}{C} - M_{24}} \tag{7}$$

where for brevity $+0$ is omitted. Inserting (7) into first and third lines of (3) with $[a,b] = [0,T]$ (see also (4) and (6)) yields:

$$\boldsymbol{\zeta}(T) = \mathbf{m}_{3\times3}\boldsymbol{\zeta}(0), \quad \boldsymbol{\zeta} = \begin{pmatrix} \boldsymbol{\xi} \\ F \end{pmatrix}, \quad \boldsymbol{\xi} = \begin{pmatrix} u \\ \sigma \end{pmatrix} \tag{8}$$

with the 3×3 matrix

$$\mathbf{m}_{3\times3} \equiv \begin{pmatrix} \mathbf{m} & \mathbf{h} \\ \mathbf{0}_{1\times2} & 1 \end{pmatrix}, \quad \mathbf{0}_{1\times2} = (0 \quad 0), \quad \mathbf{h} = \frac{1}{\frac{S}{C} - M_{24}}\begin{pmatrix} M_{14} \\ M_{21} \end{pmatrix} \tag{9}$$

where $\mathbf{m}$ is 2×2 propagator

$$\mathbf{m} \equiv \begin{pmatrix} M_{11} & M_{13} \\ M_{31} & M_{11} \end{pmatrix} + \frac{1}{\frac{S}{C} - M_{24}}\begin{pmatrix} M_{14} \\ M_{21} \end{pmatrix}\begin{pmatrix} M_{21} \\ M_{14} \end{pmatrix}^{\top} \tag{10}$$

$^\top$ means transposition. The 2×2 transfer matrix $\mathbf{m}$ plays the same role as the transfer matrix through an elastic medium because it acts on the elastic vector $\boldsymbol{\xi}$ (8). The determinant of $\mathbf{m}$ and hence of $\mathbf{m}_{3\times 3}$ is equal to 1, see details in [12]. Omitting exceptional cases of degeneracy of eigenvalues, the matrix $\mathbf{m}_{3\times 3}$ has three eigenvalues λ_j and three eigenvectors $\boldsymbol{\zeta}_j$ satisfying

$$\mathbf{m}_{3\times 3}\boldsymbol{\zeta}_j=\lambda_j\boldsymbol{\zeta}_j,\quad j=1,2,3 \tag{11}$$

These eigenvalues and eigenvectors are

$$\lambda_1=\mathrm{e}^{\mathrm{i}KT},\quad \lambda_2=\mathrm{e}^{-\mathrm{i}KT},\quad \boldsymbol{\zeta}_1=\begin{pmatrix}\boldsymbol{\xi}_1\\0\end{pmatrix},\quad \boldsymbol{\zeta}_2=\begin{pmatrix}\boldsymbol{\xi}_2\\0\end{pmatrix} \tag{12}$$

$$\lambda_3=1,\quad \boldsymbol{\zeta}_3=\begin{pmatrix}\boldsymbol{\xi}_3\\1\end{pmatrix},\quad \boldsymbol{\xi}_3=(\mathbf{I}-\mathbf{m})^{-1}\mathbf{h} \tag{13}$$

where $\mathbf{I}$ is the identity matrix, $\lambda_{1,2}$ and $\boldsymbol{\xi}_{1,2}$ are eigenvalues and eigenvectors of $\mathbf{m}$ and $K=-\mathrm{i}\log(\lambda_1)/T$ is the wave number. Using the fact that the sum of the eigenvalues is just the trace of the matrix, we obtain a simple dispersion equation expressing the dependence of the wave number K on the frequency ω:

$$2\cos KT=\mathrm{Trace}(\mathbf{m}) \tag{14}$$

or (see (10) and (4))

$$\cos KT=M_{11}+\frac{M_{14}M_{21}}{\frac{S}{C}-M_{24}}\ \Rightarrow\ \cos KT=\frac{\left(\frac{S}{C}+\frac{T}{\varepsilon}\right)\cos kT-\frac{h^2\sin kT}{Z}}{\frac{S}{C}+\frac{T}{\varepsilon}-\frac{h^2\sin kT}{Z}} \tag{15}$$

Note that a different derivation of the dispersion equation (15) was given in [11]. The edges of stopbands are defined by equation (15) with $\cos KT=\pm 1$, which corresponds to the periodic and antiperiodic solutions (center and edges of the Brillouin zone). According to [11], the solutions of equation (15) with $\cos KT=1$ are $kT=2\pi n$, $n=0,1,2,\dots$ and the solutions of equation (15) with $\cos KT=-1$ are

$$kT=\pi+2\pi n,\ n=0,1,2,\dots\ \text{ and }\ \tan\frac{kT}{2}=\beta\frac{kT}{2}\ \text{ with }\ \beta=\left(\frac{S}{C}+\frac{T}{\varepsilon}\right)\frac{c^{\mathrm{D}}}{h^2T} \tag{16}$$

where it is assumed that $k\neq 0$ and $\beta\neq 0$ (the special case $\beta=0\ \Leftrightarrow\ C=C_\infty=-\varepsilon S/T$ is considered in Section 3). Note that the matrix $\mathbf{m}$ is the identity matrix at $kT=2\pi n\neq 0$ (while it has the Jordan form at $kT=0$ and $kT=\pi+2\pi n$). According to the general theory [22], this means that the open stopbands never arise at the center of the Brillouin zone $KT=0$ except for the quasistatic stopband (see Section 3).

Let us discuss the solutions with initial data $\boldsymbol{\zeta}(0)=\boldsymbol{\zeta}_j$, $j=1,2,3$. For $j=3$ we have that $\boldsymbol{\zeta}(T)=\boldsymbol{\zeta}(0)$ and hence the corresponding solution $\boldsymbol{\zeta}$ is periodic. So the components u,σ,F and hence D, $\varphi(\cdot+T)-\varphi(\cdot)$ (6) are also periodic. It is also obvious that $\varphi(T)-\varphi(0)\neq 0$ because otherwise, i.e. if $\varphi(T)-\varphi(0)=0$, then $D(0)=D(T)=C/S$ (see (6) with $F=1$) and the vector $(u(0)\ \varphi(0)\ \sigma(0)\ D(0))^\top$ is an eigenvector of $\mathbf{M}_{4\times 4}$ (4) corresponding to an eigenvalue of 1. This is a contradiction because the matrix $\mathbf{Q}$ (2) does not have eigenvectors with a non-zero fourth component corresponding to an eigenvalue of 0, and hence $\mathbf{M}_{4\times 4}=\exp(T\mathbf{Q})$ neither have eigenvalues with a non-zero fourth component corresponding to an eigenvalue of 1. Thus we have $\varphi(T)-\varphi(0)\neq 0$ and therefore the value

$$\varphi(nT)-\varphi(0)=\varphi(nT)-\varphi((n-1)T)+\ldots+\varphi(T)-\varphi(0)=n(\varphi(T)-\varphi(0)) \tag{17}$$

tends to ∞ for $n\to\infty$ which means that φ has infinite linear growth.

Now consider the solution with initial data $\boldsymbol{\zeta}(0)=\boldsymbol{\zeta}_j$, $j=1,2$. Let $\mathrm{Im}(KT)\neq 0$. Then because $|\mathrm{e}^{\mathrm{i}KT}|>1$ or $|\mathrm{e}^{\mathrm{i}KT}|<1$, this solution $\boldsymbol{\zeta}(nT)$ and hence the components u,σ,φ,D have exponential growth for $n\to\infty$ or $n\to-\infty$. Next, let $\mathrm{Im}KT=0$ and $\mathrm{e}^{\mathrm{i}KT}\neq 1$. Then the solution with initial data $\boldsymbol{\zeta}(0)=\boldsymbol{\zeta}_j$, $j=1,2$ has quasiperiodic and bounded components $u,\sigma,F=0$ and D (see (7)) and a bounded component φ because

$$\begin{aligned}\varphi(nT)-\varphi(0)&=\varphi(nT)-\varphi((n-1)T)+\ldots+\varphi(T)-\varphi(0)\\&=(\varphi(T)-\varphi(0))\sum_{j=0}^{n}\mathrm{e}^{\mathrm{i}jKT}=(\varphi(T)-\varphi(0))\frac{\mathrm{e}^{\mathrm{i}(n+1)KT}-1}{\mathrm{e}^{\mathrm{i}KT}-1}\end{aligned} \tag{18}$$

Finally let $\mathrm{e}^{\mathrm{i}KT}=1$. Then $kT=2\pi n$ and the matrix $\mathbf{m}$ is the identity matrix (unless $k=0$ for $C\neq C_\infty$). Thus $\mathbf{m}$ has two linearly independent eigenvectors $\boldsymbol{\xi}_1$ and $\boldsymbol{\xi}_2$ corresponding to an eigenvalue of 1. We can construct the solution $\boldsymbol{\xi}=\alpha_1\boldsymbol{\xi}_1+\alpha_2\boldsymbol{\xi}_2$ for which $u(0)=0(=u(T))$ and hence $D(0)=0(=D(T))$ (see (7) with $M_{14}=0$ and $F=0$). Then, according to (6), $\varphi(T)=\varphi(0)$, which leads to the periodic solution $(u,\varphi,\sigma,D)^\top$.

In summary, extending the above remarks to the solutions with any initial data $\boldsymbol{\zeta}(0)=\sum_{j=1}^{3}\alpha_j\boldsymbol{\zeta}_j$, $\alpha_j\in\mathbb{C}$, we may conclude that if $\mathrm{Im}KT\neq 0$ then all solutions are unbounded and hence the corresponding frequency $\omega(KT)$ lies in a stopband.

On the other hand, if $\mathrm{Im}KT = 0$, then there exists a non-trivial bounded solution with initial data $\boldsymbol{\zeta}(0) = \sum_{j=1}^{2} \alpha_j \boldsymbol{\zeta}_j$ and hence the corresponding frequency $\omega(KT)$ lies in a passband. This conclusion is expectable indeed, but not obvious because our problem involves a 4×4 propagator matrix, whereas the spectrum is expressed in terms of dispersion curves (14) corresponding to a 2×2 propagator matrix.

3. Special features of the spectrum $\omega(KT)$ at $C < 0$

Consider the solutions of (16_2) in detail for $C < 0$ (recall that the case of negative C values lies beyond the scope of [11]). Denote all positive solutions of (16_2) as $0 < k_1 T < k_2 T < \ldots$. For large n, they have the following asymptotics

$$k_n T = \begin{cases} \pi(2n-1) - \frac{4}{\beta\pi(2n-1)} + O\left(\frac{1}{n^2}\right), & \beta < 0 \text{ or } \beta > 1 \\ \pi(2n+1) - \frac{4}{\beta\pi(2n+1)} + O\left(\frac{1}{n^2}\right), & 0 < \beta \le 1 \end{cases} \tag{19}$$

Invoking (16_1), all stopbands γ_n (where $\mathrm{Im}KT \neq 0$) lying above the first dispersion branch can be expressed in terms of kT as follows:

$$\gamma_n = \begin{cases} (\pi(2n-1), k_n T), & \beta < 0 \Leftrightarrow C_\infty < C < 0 \\ (k_n T, \pi(2n+1)), & 0 < \beta \le 1 \Leftrightarrow C_0 \le C < C_\infty \\ (k_n T, \pi(2n-1)), & \beta > 1 \Leftrightarrow C < C_0 \text{ or } C > 0 \end{cases} \tag{20}$$

where $n \ge 1$ and

$$\frac{C_0}{S} = -\frac{\varepsilon c^{\mathrm{D}}}{T c^{\mathrm{E}}} = -\frac{\varepsilon}{T}(1+\varkappa^2), \quad \frac{C_\infty}{S} = -\frac{\varepsilon}{T} \tag{21}$$

where $\varkappa^2 = \frac{e^2}{\varepsilon c^{\mathrm{E}}}$ is the squared piezoelectric coupling coefficient as defined in [23]. In addition there is the quasistatic stopband

$$\gamma_0 = (0, \pi) \quad \text{for} \quad C_0 \le C < C_\infty \tag{22}$$

The edges of all stopbands γ_n, $n \ge 1$ and the upper edge of the quasistatic stopband γ_0 correspond to $KT = \pi$ while the lower edge $\omega = 0$ of the quasistatic stopband corresponds to $KT = 0$.

Another approach to visualize the arrival of the quasistatic stopband is based on the analysis of the quasistatic effective elastic constant. Substituting asymptotics (see (4))

$$M_{11}(\omega) = 1 - \frac{T\rho\omega^2}{2(c^D)^2} + O(\omega^4), \quad M_{14}(\omega) = \frac{eT}{\varepsilon c^D} + O(\omega^2) \tag{23}$$

$$M_{21}(\omega) = \frac{-Te\rho\omega^2}{2\varepsilon(c^D)^2} + O(\omega^4), \quad M_{24}(\omega) = \frac{T(e^2 - \varepsilon c^D)}{\varepsilon^2} + O(\omega^2) \tag{24}$$

into the dispersion equation (15) leads to the following quasistatic limit

$$v = \lim_{K\to 0} \frac{\omega}{K} = \sqrt{\frac{c^0_{\mathrm{eff}}}{\rho_{\mathrm{eff}}}} \quad \text{with} \quad c^0_{\mathrm{eff}} = c^{\mathrm{E}} + \frac{e^2}{\frac{CT}{S} + \varepsilon}, \quad \rho_{\mathrm{eff}} = \rho \tag{25}$$

It is seen from (25) that c^0_{eff} is negative for the interval $C \in (C_0, C_\infty)$ where C_0 and C_∞ introduced in (21) are zero and pole of c^0_{eff}, respectively. This leads to a quasistatic absolute stopband that starts from $kT = 0$ ($\omega = 0$) and extends to $kT = \pi$.

The value $C = C_\infty = -S\varepsilon/T$, which is when the external capacitance C is equal to minus the capacitance of the layer, is the special one for our problem. Inserting $C = C_\infty$ into (15) reduces the dispersion equation to the form $\cos KT = 1$, hence the solution $\omega(KT)$ degenerates for $C = C_\infty$ to the value $KT = 0$ at any ω. Note that the monodromy matrix $\mathbf{m}$ at $C = C_\infty$ has the lower Jordan form for all ω such that $kT \neq 2\pi n$, $n = 0, 1, 2, \ldots$ and hence $\mathbf{m}$ has only one eigenvector $\boldsymbol{\xi}_1$ with $u(0) = 0$, $\sigma(0) \neq 0$. This yields $\varphi(T) \neq \varphi(0)$ (see (7) and (6) with $F(0) = 0$) and then the potential has an unbounded linear growth $\varphi(nT) \to \infty$ (see (17)). Therefore the degenerate solution $KT = 0$ at any ω, which arises at $C = C_\infty$, does not belong to the propagative spectrum, except for the set of points $kT = 2\pi n$, $n = 0, 1, 2, \ldots$.

Another remarkable feature of the spectrum at $C < 0$ is the occurrence of the poles of $\mathrm{Im}KT$ and the corresponding jumps of the phase $\mathrm{Re}KT$ from 0 to π in the stopbands. According to Eq. (15), the poles of $\mathrm{Im}KT$ are associated with the poles of the monodromy matrix $\mathbf{m}$, which come about at $S/C - M_{24} = 0$ unless $C = C_\infty$ (then $S/C - M_{24} = -hM_{14}$ and zeros of the denominator and the numerator in Eq. (15) occur at the same value $M_{14} = 0$, i.e. $kT = \pi n$). With reference to (4), the equality $S/C = M_{24}$ yields the following equation on the poles

$$R(\omega) \equiv \frac{\sin kT}{kT} = \beta \tag{26}$$

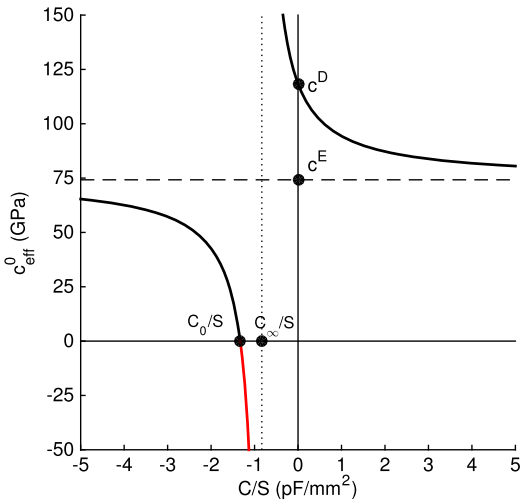

Fig. 3. (Color online.) Dependence of the quasistatic effective elastic constant $c^0_{\rm eff}$ on the external capacitance C for the PZT periodically layered structure depicted in Fig. 1.

where β is defined in (16). The frequencies ω_n and the corresponding capacitances C_n of the appearances and disappearances of poles are exactly the points where the graph of the function on the left-hand side (26) is tangent to the horizontal line on the right-hand side. Thus the frequencies ω_n of appearance and disappearance of the poles are, respectively, the (negative) minima and (positive) maxima of the function $R(\omega)$. After a new pole arrives at a minimum of $R(\omega)$, it splits into two ones with further decrease of C. The local extremes ω_n of $R(\omega_n)$ can be found explicitly. Denoting the roots of the equation $\tan x = x$ by x_n, $n = 0, 1, \ldots$:

$$x_0 = 0, \quad x_1 \approx 4.5002, \ \ldots\ , \quad x_n = \frac{\pi(2n-1)}{2} - \frac{2}{\pi(2n-1)} + O\left(\frac{1}{n^2}\right), \ \ldots \tag{27}$$

we obtain that $kT = x_n$ or

$$\omega_n = \frac{x_n}{T}\sqrt{\frac{c^D}{\rho}} \ \Rightarrow\ C_n = \frac{S\varepsilon}{\frac{Te^2}{\varepsilon c^D}\frac{\sin x_n}{x_n} - T} \tag{28}$$

Note that the global maximum and minimum of $R(\omega)$ are $R(\omega_0)$ and $R(\omega_1)$. Hence using (26) and (28) we always have at least one pole for given C if and only if

$$C_0 < C < C_1 (< 0) \tag{29}$$

where C_0 is first introduced in (21_1). Thus, as the capacitance C decreases from 0, the first pole appears at ω_1 for the capacitance C_1. After that new poles appear at higher frequencies ω_{2n+1} for the capacitances C_{2n+1} (note that $C_1 > C_3 > \ldots$). As $C \to C_\infty$, the number of poles increases (but stays finite) and they tend to the points $kT = \pi n$. This creates quasiflat passbands lying between $kT = 2\pi n$ and the neighboring poles. Recall that at $C = C_\infty$ the solution of the dispersion equation degenerates to the straight line $KT = 0$ at any ω, so all the poles merge with points $kT = \pi n$ and disappear. For the capacitances $C_{2n} < C_\infty$, the poles arrive again and begin to disappear one by one starting from large frequencies ω_{2n} because $C_0 < C_2 < \ldots$ The last pole disappears at $\omega_0 = 0$ for the capacitance C_0, see Eq. (29). Recall that C_0 is exactly the value at which the quasistatic stopband vanishes. If $C < C_0$, then there are no poles.

4. Example

Following [10,11], consider an example of the PZT periodically layered structure where each PZT layer is electroded and connected as shown in Fig. 2. Let $T = 10$ mm. The material constants taken from [10,11] are

$$e = 19.2\ \mathrm{N/V\cdot m}, \quad \varepsilon = 8.33\ 10^{-9}\ \mathrm{F/m}, \quad c^E = 7.421\ 10^{10}\ \mathrm{N/m^2}, \quad \rho = 7500\ \mathrm{kg/m^3}$$

The dependence (25) of the quasistatic effective elastic constant $c^0_{\rm eff}$ on C is plotted in Fig. 3. The value $c^0_{\rm eff}$ is negative for $C/S \in (C_0/S,\ C_\infty/S)$ where $C_0/S \approx -1.3295$ pF/mm^2, $C_\infty/S = -0.833$ pF/mm^2 (see (21)).

Fig. 4 presents the low-frequency part of the dispersion spectra $\omega(KT)$ for various $C < 0$ that are compared with the trivial spectrum $\cos KT = \cos kT$ of the electrically open case $C = 0$. First of all, we note that the points $kT = \pi + 2\pi n \Rightarrow KT = \pi$ are located at the lower or upper edges of the stopbands for $C > C_\infty$ or $C < C_\infty$ respectively, see (20), and that

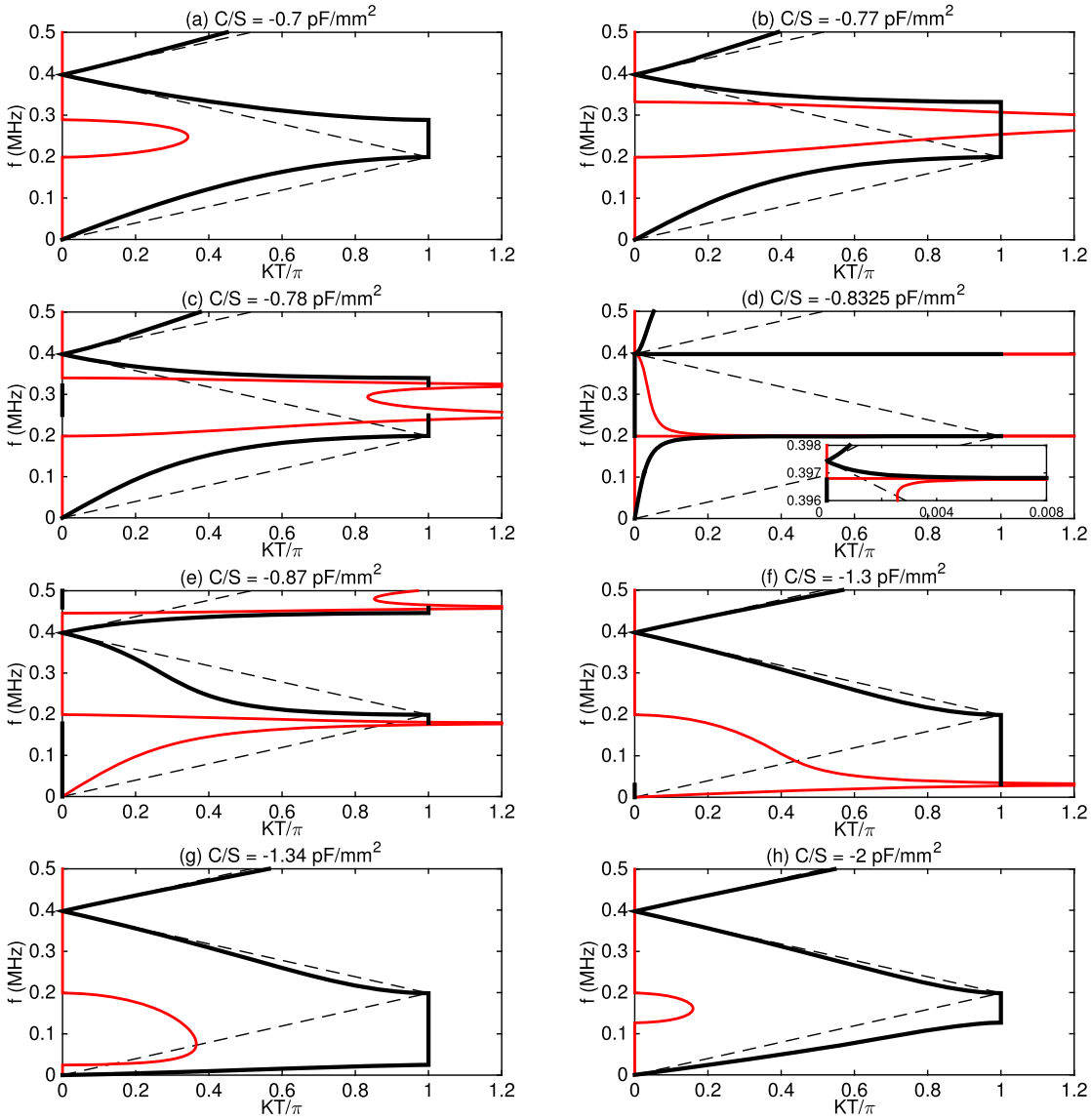

Fig. 4. (Color online.) Low-frequency dispersion curves for the PZT periodically layered structure (see Fig. 1) for various negative capacitances C. The black and red curves show ReKT and ImKT, respectively; the dashed lines indicate the spectrum for $C = 0$. The ratio v/v_0, where v is the quasistatic speed (25) of the Floquet wave and $v_0 = \sqrt{c^D/\rho} = 3974$ m/s is the reference speed of sound in the piezoelectric at $C = 0$, is equal to 1.72 (a), 2.36 (b), 2.55 (c), 24.96 (d), 0.11 (g), 0.6 (h).

there are no stopbands at $kT = 2\pi n \Leftrightarrow KT = 0$ except the quasistatic stopband. Fig. 5 shows the graphical solutions of Eq. (26) describing the appearance and disappearance of the poles of ImKT as C/S varies. Now consider the evolution of the spectra with the decrease of $C < 0$ in detail, focusing our attention on the first stopband. At $C/S \in (C_\infty/S,\ 0)$, it is located at $KT = \pi$, between the first and the second branches, see Fig. 4a. The pole of ImKT arises in the first stopband at $C_1/S \approx -0.77$ pF/mm^2, $f_1 = \omega_1/2\pi \approx 0.28$ MHz, see (28) and Figs. 4b and 5. At $C < C_1$ this pole splits into two poles that move towards the edges of the stopband along with the corresponding jumps of the phase ReKT, see Fig. 4c. As C/S approaches $C_\infty/S = -0.833$ pF/mm^2 from above (see Fig. 4d) the quasistatic phase velocity (25) and hence the group velocity $\mathrm{d}\omega/\mathrm{d}K$ of the first branch at the origin point $\omega = 0$, $K = 0$ tends to infinity. We also observe from Figs. 4d and 6 that for C tending to C_∞ from either side, all poles of ImKT and corresponding jumps of ReKT tend to the points $kT = \pi n$. This leads to quasiflat dispersion branches $\omega(KT)$ lying between the points $kT = 2\pi n$ and the neighboring poles (see in particular the inset in Fig. 4d). The group velocity of the other (not quasiflat) upper branches is finite at $KT = 0$ but tends to infinity at infinitesimally small KT as C tends to C_∞. The value $C = C_\infty$ is the special one at which c^0_{eff} is infinite and the solution of the dispersion equation degenerates to the straight line $KT = 0$. When C passes C_∞, the passbands and stopbands swap (compare Figs. 6a and 6b) and below C_∞ the quasistatic stopband γ_0 (21) arises. It starts from $\omega = 0$ and

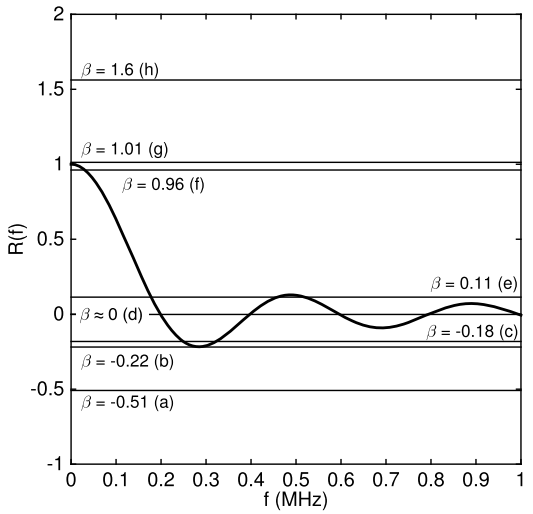

Fig. 5. Graphical solutions of eq. (26) defining the spectral positions of $\mathrm{Im}KT$ for the different values of C/S (and hence of β, see (16)) used in Fig. 4.

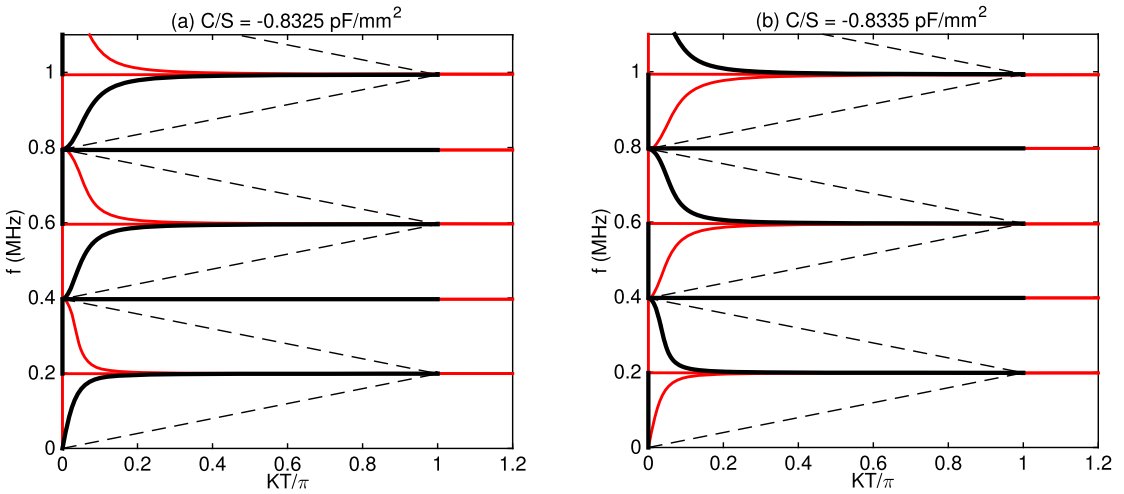

Fig. 6. (Color online.) Dispersion curves in the vicinity of the degeneracy point $C_\infty/S = -0.83$. The notations are the same as in Fig. 4.

extends to $kT = \pi$ for any C in the interval $C/S \in (C_0/S,\ C_\infty/S)$ in which $c^0_{\mathrm{eff}} < 0$ (see Fig. 3). This quasistatic stopband contains the pole of $\mathrm{Im}KT$, which is why the first dispersion branch starts at the edge of the Brillouin zone $KT = \pi$ (see Fig. 4e,f). The pole moves towards $\omega = 0$ as C tends to C_0 (see Fig. 4f). At $C/S = C_0/S \approx -1.3295$ pF/mm^2, both the quasistatic stopband and the pole of $\mathrm{Im}KT$ disappear. At $C < C_0$ the quasistatic elastic constant c^0_{eff} and hence the quasistatic phase velocity begin to grow from zero, so that the first dispersion branch reappears (first as a quasiflat branch) at its origin $\omega = 0$, $KT = 0$ (see Fig. 4g). There are no poles at $C < C_0$. Further decrease of C affects the position of the lower stopband edges (see Fig. 4h).

5. Conclusions

The dispersion spectrum $\omega(KT)$ of the longitudinal wave propagating through the periodic structure of identical piezoelectric layers, whose interfaces are electroded and connected via external electric circuits with the capacitance C, has been analyzed in the case of negative values of C. The spectrum for $C < 0$ displays a number of unusual features such as the quasistatic stopband extending from $\omega = 0$ to a certain nonzero ω, the poles of $\mathrm{Im}KT$ and corresponding jumps of $\mathrm{Re}KT$ from 0 to π, the occurrence of the infinitely growing group velocity and of the quasiflat dispersion branches. Explicit analysis of these features is facilitated by a simple form of the dispersion equation for the case of identical piezoelectric layers (a single-layered unit cell), which is why this case has been chosen for consideration. At the same time, similar spectral features can also be observed in the case of a multilayered unit cell containing elastic and electroded piezoelectric layers. The only difference in this case is that the propagator **m** through a period, whose trace appears on the right-hand side

of the dispersion equation (14), is now a product of the 2×2 propagators through individual layers. As we have seen, the propagator through each electroded piezoelectric layer has a pole for a certain $C < 0$, which leads to the pole of the aggregate propagator $\mathbf{m}$ and hence of $\mathrm{Im}KT$. Furthermore, the common physical reason for the existence of the quasistatic stopband is the negative value of the quasistatic effective elastic constant c^0_{eff}, which occurs at certain $C < 0$ for either a single-layered or a multilayered unit cell, see [13].

Finally, let us note that certain extreme features of the presented band diagrams, in particular the arbitrarily large values of the phase and group velocities in the low-frequency domain, have been obtained while considering quasistatic descriptions for the electrical network and the piezoelectric part of the structure. Specifically for such very fast electro-mechanical Floquet waves within the heterostructure, taking into account a non-quasistatic piezoelectric model and discarding the assumption of the 'instantaneous' response of the electrical network are likely to limit the caused variations in the dispersion spectrum. Nevertheless, it is shown here that the electric control of a phononic structure with the help of negative impedance allows drastic and unusual modifications of the band diagrams for a structure that was initially mechanically homogeneous.

Acknowledgements

This work was performed under the auspices of the Labex AMADEUS ANR-10-LABX-0042-AMADEUS with the help of French State "Initiative d'excellence" IdEx ANR-10-IDEX-003-02. The research was conducted in the framework of the project MIRAGES ANR-12-BS09-0015 with the support of the competitiveness cluster Aerospace Valley. The authors are grateful to A.-C. Hladky and B. Dubus for useful discussions.

References

[1] P.A. Deymier (Ed.), Acoustic Metamaterials and Phononic Crystals, Springer Series in Solid-State Sciences, vol. 173, Springer, Berlin, 2013, Chap. 8.
[2] K.L. Jim, C.W. Leung, S.T. Lau, S.H. Choy, H.L.W. Chan, Thermal tuning of phononic bandstructure in ferroelectric ceramic/epoxy phononic crystal, Appl. Phys. Lett. 94 (2009) 193501.
[3] K. Bertoldi, M.C. Boyce, Mechanically triggered transformations of phononic band gaps in periodic elastomeric structures, Phys. Rev. B 77 (2008) 052105.
[4] J.-Y. Yeh, Control analysis of the tunable phononic crystal with electrorheological material, Physica B 400 (2007) 137.
[5] J.-F. Robillard, O. Bou Matar, J.O. Vasseur, P.A. Deymier, M. Stippinger, A.-C. Hladky-Hennion, Y. Pennec, B. Djafari-Rouhani, Tunable magnetoelastic phononic crystals, Appl. Phys. Lett. 95 (2009) 124104.
[6] O. Bou Matar, J.-F. Robillard, J.O. Vasseur, A.-C. Hladky-Hennion, P.A. Deymier, P. Pernod, V. Preobrazhensky, Band gap tunability of magneto-elastic phononic crystal, J. Appl. Phys. 111 (2012) 054901.
[7] O. Thorp, M. Ruzzene, A. Baz, Attenuation and localization of wave propagation in rods with periodic shunted piezoelectric patches, Smart Mater. Struct. 10 (2001) 979.
[8] G. Wang, S. Chen, J. Wen, Low-frequency locally resonant band gaps induced by arrays of resonant shunts with Antoniou's circuit: experimental investigation on beams, Smart Mater. Struct. 20 (2011) 015026.
[9] F. Casadei, T. Delpero, A. Bergamini, P. Ermanni, M. Ruzzene, Piezoelectric resonator arrays for tunable acoustic waveguides and metamaterials, J. Appl. Phys. 112 (2012) 064902.
[10] S. Degraeve, C. Granger, B. Dubus, J.O. Vasseur, A.-C. Hladky, M. Pham-Thi, Contrôle électrique de la propagation d'ondes élastiques dans des cristaux phononiques piézoélectriques (Electric control of the propagation of elastic waves in the piezoelectric phononic crystals), in: 21e Congrès Français de Mḿecanique Bordeaux, 26–30 August 2013, http://documents.irevues.inist.fr/handle/2042/52155 (in French).
[11] S. Degraeve, C. Granger, B. Dubus, J.O. Vasseur, M. Pham Thi, A.-C. Hladky-Hennion, Bragg band gaps tunability in an homogeneous piezoelectric rod with periodic electrical boundary conditions, J. Appl. Phys. 114 (2014) 194508.
[12] A.A. Kutsenko, A.L. Shuvalov, O. Poncelet, A.N. Darinskii, Tunable effective constants of the one-dimensional piezoelectric phononic crystal with internal connected electrodes, J. Acoust. Soc. Amer. 137 (2015) 606–616.
[13] A.A. Kutsenko, A.L. Shuvalov, O. Poncelet, A.N. Darinskii, Quasistatic stopband in the spectrum of one-dimensional piezoelectric phononic crystal, http://arxiv.org/abs/1410.7215, 2014, open access.
[14] S. Degraeve, C. Granger, B. Dubus, J.O. Vasseur, M. Pham-Thi, A.-C. Hladky, Tunability of a one-dimensional elastic/piezoelectric phononic crystal using external capacitances, Acta Acust. Acust. 101 (2015) 494–501.
[15] V.S. Kshatri, J.M.C. Covington, K.L. Smith, J.W. Shehan, T.P. Weldon, R.S. Adams, Measurement and simulation of a CMOS current conveyor negative capacitor for metamaterials, in: SOUTHEASTCON 2014, 13–16 March 2014, Lexington, KY, USA, IEEE, 2014, pp. 1–5.
[16] R. Senani, D.R. Bhaskar, A.K. Singh, Current Conveyors: Variants, Applications and Hardware Implementations, Springer, Cham, Heidelberg, New York, Dordrecht, London, 2015.
[17] S.-B. Chen, J.-H. Wen, D.-L. Yu, G. Wang, X.-S. Wen, Band gap control of phononic beam with negative capacitance piezoelectric shunt, Chin. Phys. B 20 (2011) 014301.
[18] B.S. Beck, K.A. Cunefare, M. Ruzzene, M. Collet, Experimental analysis of a cantilever beam with a shunted piezoelectric periodic array, J. Intell. Mater. Syst. Struct. 22 (2011) 1177–1187.
[19] Y.Y. Chen, G.L. Huang, C.T. Sun, Band gap control in an active elastic metamaterial with negative capacitance piezoelectric shunting, J. Vib. Acoust. 136 (2014) 061008.
[20] H. Zhang, J. Wen, Y. Xiao, G. Wang, X. Wen, Sound transmission loss of metamaterial thin plates with periodic subwavelength arrays of shunted piezoelectric patches, J. Sound Vib. 343 (2015) 104–120.
[21] H. Nowotny, E. Benes, General one-dimensional treatment of the layered piezoelectric resonator with two electrodes, J. Acoust. Soc. Amer. 82 (1987) 513–521.
[22] A.A. Kutsenko, A.L. Shuvalov, O. Poncelet, A.N. Norris, Spectral properties of a 2D scalar wave equation with 1D periodic coefficients: application to shear horizontal elastic waves, Math. Mech. Solids 18 (2013) 677–700.
[23] B.A. Auld, Acoustic Fields and Waves in Solids, Vol. 2, Wiley, 1973.